The International Journal of Advanced Manufacturing Technology (2019) 105:2907–2917
https://doi.org/10.1007/s00170-019-04518-z

ORIGINAL ARTICLE

Steel subsurface damage on plunge cylindrical grinding with sol-gel aluminum oxide grinding wheels

Fernando Moreira Bordin [1] · Walter Lindolfo Weingaertner [1]

Received: 21 May 2019 / Accepted: 27 September 2019 / Published online: 9 November 2019

Abstract
Highlighted in many engineering applications, such as bearing and crankshaft grinding, cylindrical circumferential plunge grinding is a manufacturing process that encompasses multiple stages (roughing, finishing and spark-out) in a series of overlapping steps. Although this is especially a critical process when grinding with aluminum oxide abrasive grits, only a little information of the subsurface damage is available when applying microcrystalline aluminum oxide grits. In order to evaluate the influence of the microcrystalline Al_2O_3 grits content in conventional grinding wheels on the ground subsurface, grinding experiments were performed. The microcrystalline aluminum oxide abrasive grit content was varied from 15 to 45%. The morphological characteristics of the grinding wheels were analyzed via X-ray tomography. A single-step specific material removal rate (roughing condition) was selected to induce microstructural modifications on the workpiece subsurface. The grinding force was monitored, and its components were determined. The X-ray tomography revealed that with a variation of the microcrystalline aluminum oxide content, the binder proportion that classified the used and evaluated grinding wheels with the same hardness does not present the same binder content. This is a piece of information normally not present in the description of the wheels by the manufacturer and is helpful to explain behaviors on the force and affected layer, not possible only with the information of grit content and hardness. Investigating the present layers on the modified microstructure suggests the governing phenomena during cutting, and a deepening of the studies with X-ray tomography helps to explain phenomena that were not explainable before.

Keywords Cylindrical plunge grinding · Microcrystalline aluminum oxide grits · X-ray tomography · Microstructural modifications · Grinding force components

1 Introduction

Manufacturing processes compete in terms of cost, quality, time, flexibility and, recently, sustainability. In this scenario, grinding is highlighted as it spans from very crude and rough applications in cutting of materials at high material removal rates (MRR) to finishing and ultraprecision processes [1, 2]. However, in grinding, there is always a trade-off between the quality of the machined product (surface finish and integrity) and the productivity (MRR and operational cost). Selection of proper grinding wheel–workpiece combination along with process parameters such as feed rate, cutting speed, and depth of cut plays a key role in producing a high-quality product with higher productivity [3].

External cylindrical circumferential plunge grinding poses a complementary challenge from the characterization/evaluation perspective, as the surface is constantly under material removal and therefore affected by constant workpiece/grinding wheel interactions [4]. The cycles of heating and cooling that occur on the ground surface in association with several overlaps of material removal lead to cyclic changes on the material microstructure and properties [5]. The knowledge of the damage extension is a key aspect that aids in developing an effective grinding operation planning [6], as well as studies on the modeling of phase transformation after the grinding process [7].

✉ Fernando Moreira Bordin
f.m.bordin@posgrad.ufsc.br

Walter Lindolfo Weingaertner
w.l.weingaertner@ufsc.br

[1] Campus Reitor João David Ferreira Lima, Centro Tecnológico (CTC), Department of Mechanical Engineering, Bloco B, Laboratório de Mecânica de Precisão (LMP), Universidade Federal de Santa Catarina (UFSC), Trindade, Florianópolis CEP: 88040-970, Brazil

The use of microcrystalline sol-gel aluminum oxide (SG-Al_2O_3) grits in conventional vitrified grinding wheels came as an alternative, showing intermediate properties between electro-fused Al_2O_3 and cBN abrasives. The continuous development of these abrasives started in the 1960s; however, the industrial application only began recently. The differential wear behavior of this abrasive is due to the microcrystalline sintered structure, endowed with micro- and, in particular cases, nano-crystallites of Al_2O_3, granting higher toughness and wear resistance than electro-fused Al_2O_3. The higher dressing flexibility and lower cost than superabrasive abrasive grinding wheels are also a decisive factor when selecting this type of grinding wheels [8].

The focus of researches and case studies with the use of SG microcrystalline Al_2O_3 concerns about wear of grinding wheels, showing greater advantages in terms of wear resistance and efficiency (higher G-ratio) when compared to electro-fused Al_2O_3 [9–11]. Early studies have shown that the best results are associated with a higher material removal rate, due to the differentiated sol-gel grain splintering mechanism [7, 11, 12]. Brunner [13] observed, during plunge grinding of bearing steel (AISI 52100) with 100% concentration sol-gel Al_2O_3 grinding wheel, that the micro-wear changes from a severely deformed grain surface to a micro splintered surface as the specific material removal rate changes from 1 to 4 mm^3/mms. This statement was later investigated by Klocke et al. [14], during pin on disk scratching tests. The authors determined that the wear of sol-gel aluminum oxide is affected by severe plastic deformation of the outmost abrasive grain layer, involved in a complex chemical reaction and oxide layer formation, which promotes a friction reduction.

However, only a handful of authors investigated the subsurface damage on steel components caused by the presence of microcrystalline sol-gel Al_2O_3 grits on the grinding wheel structure [10, 15–17]. The evaluation performed by the authors was restricted to the surface grinding process, showcasing evaluations where only the utmost material layer is removed. In contrast, the cylindrical plunge ground surface is the target of several layers of material removal, promoting a complex phenomenon of subsurface modifications.

Usual modifications on the subsurface scale range from plastically deformed zones, martensite to ferrite/pearlite transformations, and ferrite/pearlite to martensite phase transformations. These modifications are identified as the white layer (composed of untempered martensite and retained austenite), dark layer (composed of overtempered martensite), and plastically deformed layer. The appearance of these phenomena is intrinsically correlated to the grinding process mechano-thermal and thermo-mechanical loads [18, 19].

Kitamura and Gotanda [10] evaluated the residual stress profile with an increase of the stock removal (wheel life), after surface grinding of an AISI 1055 steel. Conventional white fused and sol-gel aluminum oxide grinding wheels were used in the experiments. Results show a continuous and rapid increase in the residual stress, shifting from compressive to tensile stress for the electro-fused grinding wheel, whereas the SG grinding wheel presented a steady and small increase rate of the compressive residual stress.

In a similar approach, Fathallah et al. [15] compared the results when grinding of AISI D2 steel with conventional wheels with white fused aluminum oxide and with sol-gel aluminum oxide. The depth of the modified layer was evaluated in terms of residual stress, under several specific material removal rates (Q_w'). For an increase in the Q_w', the results show a rapid increase in the residual stress (from initial compressive to tensile) for the white fused aluminum oxide, whereas the sol-gel aluminum oxide presented a steady increase rate on the residual stress.

Madopothula et al. [16, 17] observed, when surface grinding of AISI 52100 steel with a specific material removal rate of 1.2 mm^3/mms, a higher grinding force, temperature rise, and thicker boundary-affected layer when grinding with sol-gel aluminum oxide, in comparison with white fused aluminum oxide abrasives grinding wheels.

This study aims to fill the knowledge gap of subsurface damage evaluation when using SG grinding wheels in cylindrical plunge grinding. The experiments were conducted during external cylindrical plunge grinding of an AISI 1040 steel with grinding wheels with microcrystalline Al_2O_3 content up to 45%.

2 Materials and methods

2.1 Machine-tool and experimental setup

Single-stage external cylindrical plunge grinding cycles were performed on a CNC Zema Zselics Pratika Flexa 600 L cylindrical grinding machine-tool. The grinding experiments were performed with grinding wheels, containing concentrations 85%, 70%, and 55% of electro-fused Al_2O_3 and 15%, 30%, and 45% microcrystalline sol-gel Al_2O_3 as grit balance. The steel probes were mounted on a KISTLER INSTRUMENTE AG RCD 9124B1111 rotating dynamometer on the machine's workpiece spindle (headstock). Figure 1 illustrates the overall experimental setup for the grinding experiments.

At the start of each grinding section (not including experiments with increasing specific material removal V_w'), the grinding wheels were dressed with a dressing disk embedded with diamond abrasive grits. The specific material removal V_w' was increased at each fixed cycle interval, in order to evaluate the wear influence on the force/energy generation and subsurface damage. Along with microstructural characterization of the ground surface, the specific grinding force components, tangential F_t' and normal F_n', were calculated.

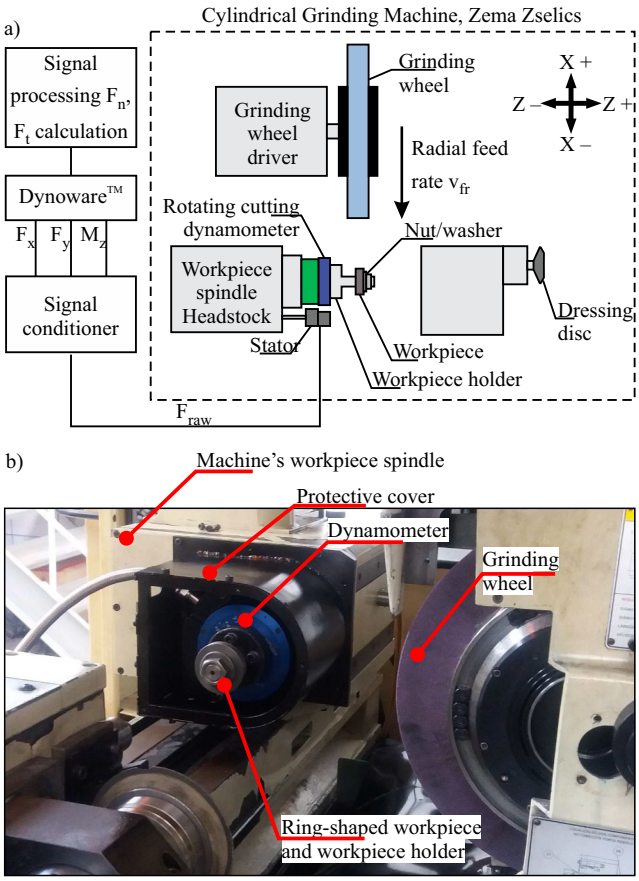

Fig. 1 Experimental setup for the experiments: **a** schematic illustration and **b** detailed view of the grinding machine and grinding force measuring system

Table 1 details the input and system parameters employed during the experiments.

The radial feed rate v_{fr} increased as the workpiece diameter (d_w) decreased, in order to keep the specific material removal rate constant. In favor of evaluating the respective subsurface damage at each specific material removal rate, the grinding cycle was performed without spark-out time, through quick reversion of infeed motion.

The evaluation of the subsurface damage was performed by increasing the specific material removal interval up to $V_w' = 1000\ mm^3/mm$ or intense noise due to vibration on the process. The latter criterion was adopted due to the low stiffness of the force measurement system, characterized by intense chatter.

2.2 Tool and workpiece

2.2.1 Grinding wheel

The grinding wheels presented an initial geometry of 400 mm × 203.2 mm × 30 mm, with average abrasive grain size FEPA 80 (~ 185 μm), hardness J, porosity 6, and vitreous bond produced specifically for the ongoing research project by *Krebs & Riedel*, Germany, with an SG microcrystalline Al_2O_3 grit content of 15%, 30%, and 45%, denominated MC15, MC30, and MC45 respectively. The grinding wheels were characterized in terms of structure/phase fraction (binder, pores, abrasive grits) as a means to compare the input information from the manufacturer and observe the phase distribution. This analysis was performed using X-ray microtomography technique, using a Versa XRM-500 tomographer. The image acquisition parameters for the computer microtomography are shown in Table 2.

Cylindrical probes with 4-mm diameter and 10-mm length of the samples were trepanned out of the grinding wheel periphery and characterized in terms of phase distribution using the software Avizo and Imago. The phases were segmented into separated images, and the overall fraction of the phases was measured along the cylindrical sample length and is depicted in Table 3.

Table 1 Input and system parameters

Grinding wheel geometry/specification	[mm]	400 × 203.2 × 30/A80J6V
Grinding wheel peripheral speed v_s	[m/s]	30
Workpiece peripheral speed v_w	[m/min]	30
Specific material removal rate Q_w'	[mm^3/mms]	4, 5, 6
Specific material removal V_w'	[mm^3/mm]	50, 200, 500, 1000
Width of cut a_p	[mm]	10
Dressing overlap ratio U_d		1
Dressing depth a_{ed}	[μm]	10
Effective dressing width b_d	[mm]	0.8
Total dressing depth	[mm]	0.2
Cutting fluid		Ecocool AP 71
Cutting fluid application method		Flooding
Cutting fluid concentration	[%]	3
Cutting fluid flow	[l/min]	20

Table 2 X-ray microtomography acquisition parameters

Technique (scale)	Microtomography
Resolution (image pixel size)	3.83 μm
Image size	988 px × 1011 px
Camera binning	2
Font	60 kV/5 W
Exposition time	5 s
Angular step	0.225°

When comparing the volumetric fraction of the binder of the three analyzed probes, the results showed that for the grinding wheel MC15 the volumetric binder content is much higher from that of the MC30 and MC45 probes. The volumetric fraction of abrasive grits (V_g) is approximately 5% lower for the MC15 sample, whereas the pore fraction (V_p) of the MC30/MC45 samples is 6% higher than the MC15. The 11% higher binder content for the MC15 wheel is believed to be an intentional manufacturing step as means to maintain the grinding wheel hardness at a similar level when comparing grinding wheel hardness by sandblasting, provided by the manufacturer. The hardness for all grinding wheels was kept at a constant magnitude of 50 GPa.

2.2.2 Workpiece

The mid-carbon steel AISI 1040 (quenched and tempered to a hardness of 370 ± 30 HV) ring-shaped workpiece probes (initial OD d_{wi} = 50 mm, ID d_{int} = 25 mm, width s: 10 mm) component, shaped to fit on the Kistler AG dynamometer (Fig. 2).

Table 3 Average volumetric phase fraction concentration according to different grinding wheels

Sample	Phase	Phase fraction (%)	Connected phase* (%)
MC15	microcrystalline	6.7	-
	monocrystalline	43.1	98.0
	binder	21.5	98.6
	pore	28.6	98.3
MC30	microcrystalline	16.4	27.4
	monocrystalline	37.9	98.5
	binder	9.3	73.6
	pore	33.8	98.7
MC45	microcrystalline	21.8	85.1
	monocrystalline	33.1	96.7
	binder	10.3	73.3
	pore	34.8	99.3

*This is the fraction of the percolant phase. Even if the phase permeates the sample, a small portion (in most cases) remains isolated

The workpiece matrix is composed of tempered martensite, indicating little content of free ferrite (white regions).

2.3 Force measurement

Grinding force components F_n and F_t were deduced from the measured the grinding force components F_x, F_y, and moment M_z with a shielded *Kistler Instrumente AG* piezoelectric dynamometer RCD 9124B1111, shaped as a workpiece-holder, a stator 5221B, and multi-channel signal conditioner 5223B2 mounted on the machine's headstock spindle, and the workpiece was fixed on the dynamometer (Fig. 3).

The electric dynamometer signals were processed with a built-in low-pass filter of 1 kHz (according to the equipment manufacturer's manual). For the grinding force component's calculation, an average workpiece diameter was considered (considering the workpiece initial and final diameter).

The electric signals were processed with the aid of MATLAB®'s interface and toolbox, applying a low-pass equiripple filter of 58 Hz. A region of interest of the measured signal was selected and employed to determine the average and standard deviation values for the force components.

2.4 Subsurface damage analysis

The subsurface damage was characterized through optical microscopy of the transversal section of the workpiece. The images were obtained using an Olympus BX60M optical microscope, in combination with a Leica application Suite LAS EZ software. The ring-shaped samples were sectioned in four sections (90° apart) and embedded in a thermosetting phenol formaldehyde resin (Bakelite - $(C_6H_6O{\cdot}CH_2O)n$). Samples were sanded with decreasing SiC grit size abrasive papers (mesh # 80, 150, 200, 320, 400, 600, and 1200), polished with an aqueous suspension of 0.3 μm grit Al_2O_3 and etched with a Nital 2% (nitric acid + alcohol) for microstructural revelation.

Two micrographic photos of each section were selected and processed with an open-source image processing software (FIJI). A Trainable Weka Segmentation plugin, developed by Arganda-Carreras et al. [20], which combines a collection of machine learning algorithms with a set of selected image features to produce pixel-based segmentation, was used to segment different regions of the obtained metallographic photography. For each section analyzed, a color segmented image was obtained and then processed (Fig. 4). The area of each segmented feature was divided by the image width, calculating the average thickness of the boundary-affected layer (BAL).

Along with the quantitative evaluation of the alterations, a qualitative evaluation, based purely on observation, was conducted. The following features were observed: the presence of white layer (untempered martensite UTM) and the presence of dark layer (overtempered martensite OTM). These

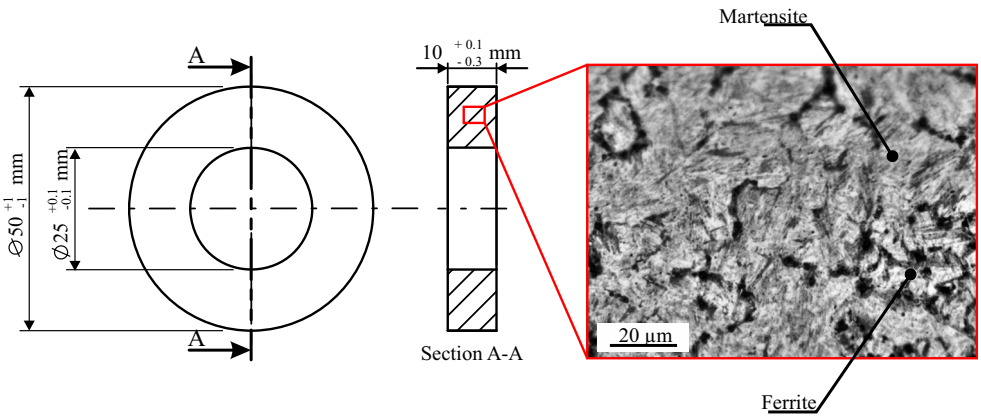

Fig. 2 Workpiece geometry and microstructure

characteristics were evaluated in terms of a binary observation: 0 for a section without the feature and 1 for a section with the feature.

3 Results and discussion

3.1 Grinding force components

The grinding force components reflect the overall process, especially the abrasive grain wear behavior. Monitoring grinding force allows concluding about the energy generation on the cutting zone and, therefore, understanding material alterations. In this scenario, Fig. 5 shows the behavior of the specific grinding force components along the specific grinding volume when grinding the AISI 1040 steel probes with the employed grinding wheels and the specific material removal rates.

It is observed that, when increasing the specific material removal along the grinding operation, there is a quasi-proportional increase of the grinding force components at the beginning. This is also stated in the literature. During grinding, the abrasive wear of the most protuse grits increases the number of kinematic cutting edges (i.e., decreasing the effective chip thickness in the cutting direction and increasing the sum of the contact length in the cutting direction) and thus increasing the force components. Due to an increase in material removal, the increase of the grinding force leads to more intense noise and chattering. Chattering was defined as the end of the grinding wheel life.

By employing a Q_w' 4 mm^3/mms, an increase of microcrystalline grits from 15 to 30 and 45% shows a significant increase of the ground volume, without detection of chattering.

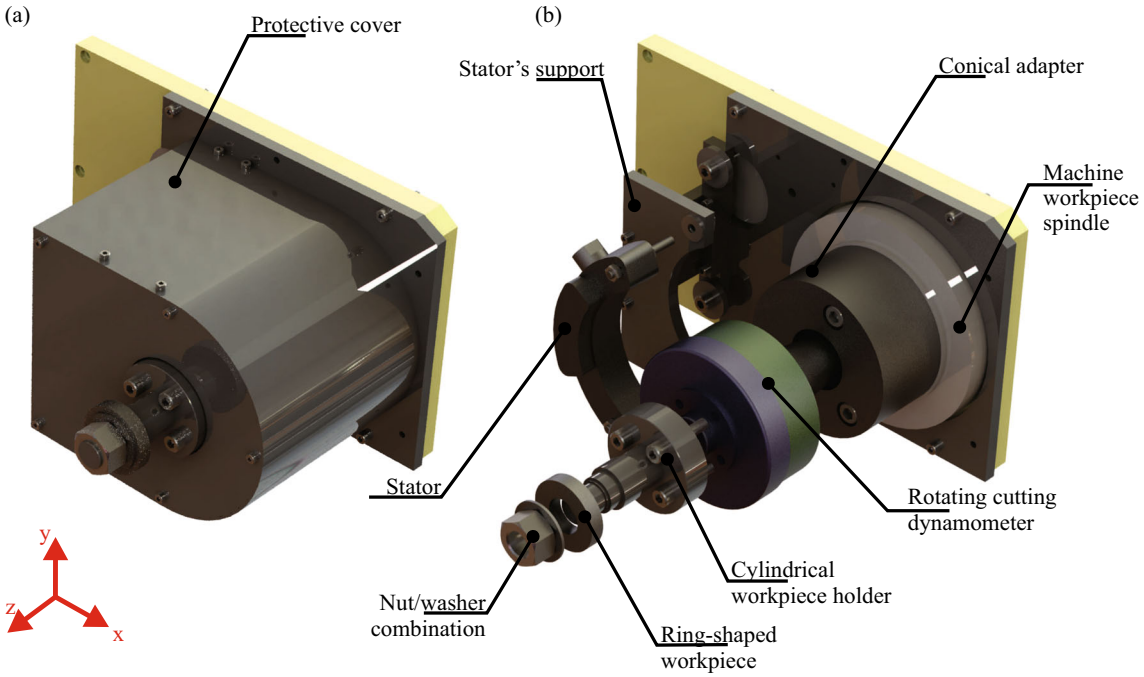

Fig. 3 Force measuring system: assembly (**a**) and detailed exploded view (**b**)

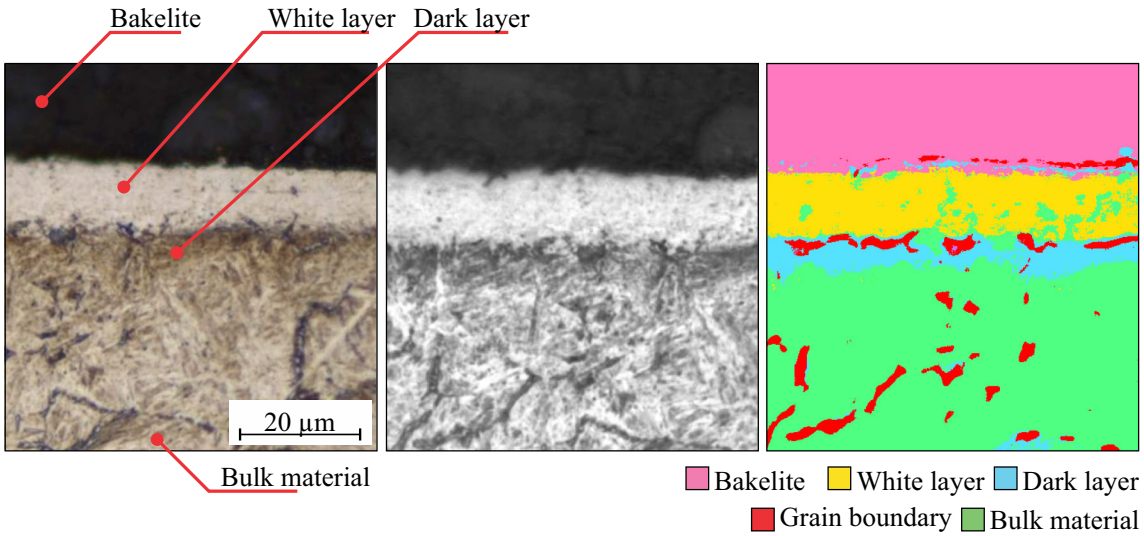

Fig. 4 Contrast-enhanced micrography: original image (**a**), grayscale image (**b**), and color segmented map (**c**)

The established ground volume of V_w' of 1000 mm^3/mm was reached while grinding force components were still in the comfortable region.

Increasing the specific material removal rate Q_w', from 4 to 5, and 5 to 6 mm^3/mms, the depth of cut a_e, consequently, the undeformed chip thickness h_{cu} and number of cutting edges N_{kin} increases, leading to higher grinding forces. The load on the grit is more intense; the grinding wheel grits present higher wear rate and a shorter life. All the experiments were interrupted because of chattering. When grinding with Q_w' of 5 mm^3/mms, the MC45 showed superior results than MC30. For Q_w' = 6 mm^3/mms, the results for MC30 and MC45 did not evidence any difference in the force measurements.

The presence of microcrystalline Al_2O_3 on the grinding wheel structure led to a few particular behaviors: for a Q_w' of 4 mm^3/mms, MC15 grinding wheel exhibited slightly higher forces than MC30 and MC45; for a Q_w' of 5, MC15 and MC30 presented slightly higher forces than MC45; and for a Q_w' = 6 mm^3/mms, there are no statistical differences between the grinding wheels.

While the grinding force components presented statistically similar values between microcrystalline contents, grinding wheels with higher content of MC grits presented longer grinding wheel life, owing to the fact that for a similar loading condition, MC grits do not splitter as electro-fused Al_2O_3 and keep a stable cutting condition along the grinding wheel life [13].

Since the dominant abrasives for all the grinding wheels are of the monocrystalline type, a similar grinding force magnitude was expected for the MC15. The early increase of the cutting forces for the MC15 wheel is influenced by the higher content of binder as for the MC30 and MC45 wheels. The MC15 wheel presents higher micro-wear than the other two wheels and, due to flatting of the grits, leads to early chattering for the three analyzed grinding rates (Q_w'). The higher binder content hinders the monocrystalline abrasive grit splintering, leading to an early chatter. Also, the discrepancy in the volumetric fraction of the phases points out that the higher concentration of abrasive grits (and the kinematic cutting edges for that matter) are prone to reduce the chip thickness parameter and, thus, increase the grinding force.

Additionally, the binding strength provided by the binder bridges on the monocrystalline and microcrystalline abrasives is different. Due to the smoother surface of the monocrystalline Al_2O_3 grit, the binder bridges have a lower real area of anchorage, whereas the microcrystalline Al_2O_3 presents a rougher surface, thus increasing the binding resistance.

In this sense, the increase in the binder content (as means to maintain the grinding wheel hardness by sandblasting) hindered the monocrystalline abrasive grit splintering, effectively increasing the grinding wheel hardness in use. In the same manner, it reduced the abrasive grit content.

In terms of abrasive grit type, studies reported by other authors illustrated an interesting behavior. Madopathula et al. [16] reported results after surface grinding, focused on finishing conditions (Q_w' of 1.2 mm^3/mms). In their study, the presence of SG grits led to an increase of the grinding force components with the increase of the specific material removal, owing to the higher toughness of the MC grits when compared with white aluminum abrasive grits.

Uhlmann et al. [21] reported, during external cylindrical plunge grinding, a decrease in the grinding force components with the increase in sol-gel alumina content. The grinding conditions selected by authors were primary roughing cycles (Q_w' of 8, 10, and 12 mm^3/mms) grinding AISI 52100 steel.

Brunner [13] calculated the critical specific normal force $F_{n,\,crit}'$, the force necessary to cause grit fracture of microcrystalline grits. The author observed, in internal cylindrical plunge grinding, that for low Q_w' (< 4 mm^3/mms), this factor

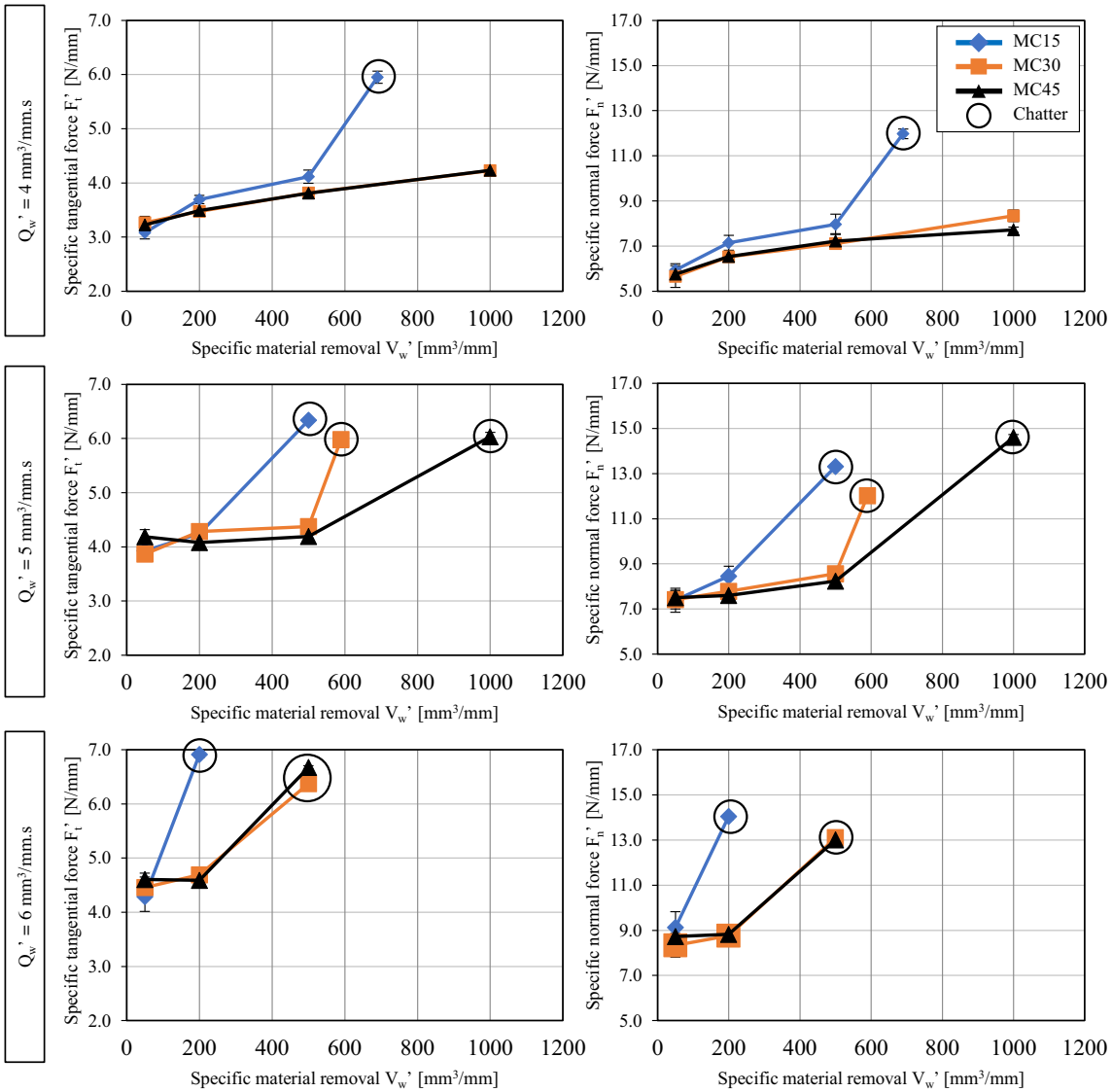

Fig. 5 Specific grinding force components with increasing material removal and sol-gel Al_2O_3 content

is high for MC Al_2O_3. As the specific normal force increases, the factor decreases, requiring less force to initiate grit fracture and, thus, lower normal forces.

The behavior of the grinding force components for the lower sol-gel content was not expected and only understood after the microtomography evaluation with an image processing procedure. This showcases the potential of microtomography tools in understanding the grinding process.

3.2 Subsurface damage

Evaluation of the subsurface damage is of major concern, whether to avoid alterations on material properties or to induce transformations on the subsurface (e.g., grind-hardening heat treatment). The knowledge of the boundary-affected layer thickness is a requirement for efficient operation planning. In this context, Fig. 6 represents the measured depth of the affected layer for the experimented conditions. The feature analysis (on the right side) describes the number of sections along the probe periphery that presented a white/dark layer.

At first glance, there is no immediate correlation between the measure boundary-affected layer thickness and the input system variables (Q_w' and V_w'), as well as the grinding force. The large dispersion of results is accounted for the nature of the cylindrical plunge grinding overlap characteristic.

There is a slight difference between the grinding wheels' ground subsurface, which implies that the type of abrasive grit involved during the surface formation had a substantial effect on the boundary-affected layer. For the lowest MC grit content, the predominance of the monocrystalline aluminum oxide is greater, which led, at the first Q_w' (4 mm^3/mms), to a BAL of 10 μm. This value decreased and then increased for the upcoming specific material removal intervals.

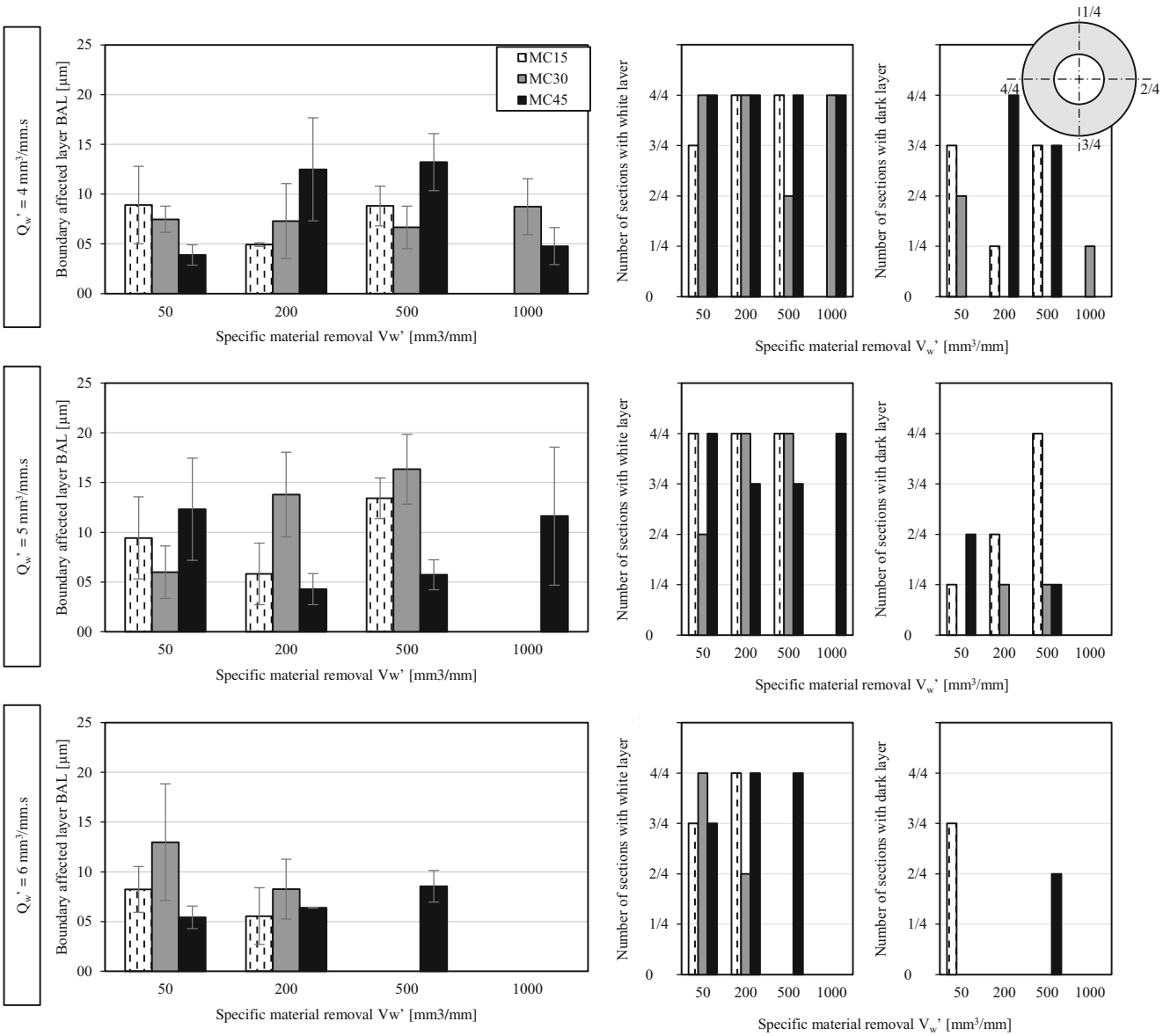

Fig. 6 Average boundary-affected layer thickness (left) and microstructure features (right)

The MC30 abrasive grit showcased a uniform formation of boundary-affected layer along the investigated sections. The higher content of MC abrasives (and less binder) led to more stable and frequent microchipping of this type of grits, leading to uniform boundary-affected layer thickness.

However, for the MC45 grinding wheel, the behavior was predominantly different. The higher presence of MC abrasive grits led to large boundary-affected layer thickness at the intermediate V_w' interval. The increase in the boundary-affected layer was associated with the presence of a dark layer, which indicates a high-temperature gradient.

For a higher specific material removal rate of 5 mm^3/mms, the MC15 illustrated an initial decrease and then increase on the BAL thickness with each volumetric interval. Since the characteristic layers are initially untempered martensite but become increasingly untempered and overtempered martensite, it is hypothesized that an increasingly intense abrasive wear took place, favoring friction.

A rapid BAL thickness increase was detected for the MC30 as the material removal increased. This was associated with only the detection of white layers. The higher content of abrasives led to early chipping of the monocrystalline grits and protrusion of the microcrystalline grits.

The MC45 illustrated an inverse behavior in comparison to the previous Q_w', with a thick initial boundary-affected layer, that reduced at the intermediate intervals, but ultimately increased at the last V_w'. Most of the microstructure phase transformations were detected as white layers; however, white layer associated with dark layer was also found at the initial interval.

For a Q_w' of 6 mm^3/mms, the MC15 and MC30 presented an initial thicker boundary-affected layer that decreased at the last volumetric interval. The MC45 demonstrated a constant BAL magnitude. The presence of the dark layer was detected for the initial MC15 volumetric interval and for the last grinding interval of the MC45 subsurface.

It is important to state that the mechanism of white layer formation is a topic of the ongoing investigation. Base literature explains that the formation of such layer is due to several mechanisms, and the structure itself is referenced as untempered martensite with the dispersion of retained austenite [18]. In grinding, these mechanisms are influenced by the thermal and mechanical severity of the process.

An intense plastic deformation leads to a large motion of discordances and atom displacements. Since the region closest to the border is under the heaviest shearing load, the microstructure deforms to the point where there is a grain refinement, causing the layer to appear under optical microscopy as a bland and blank [22, 23]. In some cases, it was also detected the presence of twinning due to the heavy plastic deformation [19]. This mechanism also aids to increase the free energy for material transformation, reducing the necessary thermal energy for phase transformation [19].

Additionally, the intense heat generated by the grinding process leads to a local temperature rise. If the workpiece temperature reaches magnitudes above the austenitization point (Ac3) and is quickly cooled below the martensite finish point (M_f), the resulting structure is martensite in nature [22–24]. This phenomenon in grinding is achieved by the self-quenching mechanism, where the high-temperature gradient caused by small layer under removal and the surrounding workpiece leads to high heat flux to the material interior (self-quenching) [22, 23], provided that the cutting fluid does not reach the cutting zone. Since the grinding contact time is short, there is not a time for grain growth, causing the structure to be nanometric in scale and, therefore, blank/featureless under optical microscopy [19].

In contrast, dark layers in steels are often referenced as overtempered martensite layers. If the heat on the subsurface is high enough to cause a temperature increase above the previous tempering point, tempering will occur [22, 23].

Several mechanisms affected the boundary-affected layer formation. Since no correlation between the grinding forces and the boundary-affected layer could be drawn, a few hypotheses were taken into consideration:

Abrasive grit wear, which implies that for a lower Q_w', a predominance of abrasion wear and grit flattening (which favors friction/rubbing), whereas in increasing the Q_w', the wear mechanism shifts to microchipping, with cutting edge renewal (self-sharpening), favoring the cutting [25, 26].

Cylindrical plunge grinding characteristics: at each possible complete rotation of the workpiece, the temperature rises to a certain peak, cools down, and rises again on the next cycle. Since the new initial temperature of the workpiece is different from the ambient temperature, it is expected that heat does not conduct fast enough, and therefore, temperature maintains within the workpiece. This cyclic behavior is also true when concerning the microstructural alterations on the boundary-affected layer, evidenced by the cyclic temperatures above and below the austenitization temperature (Ac3), causing quench and tempering effects [5].

Since the depth of the boundary-affected layer is consistently thicker than the depth of cut, a portion of the ground surface is affected by the overlapping of microstructure changing events, governed by the number of rotations. The constant changing of ground surfaces may induce to an uneven boundary-affected layer thickness.

Microcrystalline (sol-gel) Al_2O_3 grit properties: it was hypothesized by Klocke et al. [14] and Mayer et al. [12] that the higher concentration of imperfections in sol-gel corundum reduces the mean optical path length of the phonons (fundamentals packets of energy exchanged during lattice vibrations), resulting in lower heat conductivity. This leads to a spike in the temperature on the conditions of higher microcrystalline abrasive content.

Grinding wheel volumetric content: the microtomography analysis revealed discrepancies on the volumetric phase fraction (grits, pores, and binder). By increasing the volumetric binder fraction, the splintering of the monocrystalline abrasives is hindered by the binding system. Increasing the number of grits (MC30 and MC45) increases the kinematic cutting edge number, decreasing the chip thickness. This leads to higher shearing forces and, consequently, higher discordances dislocations.

Therefore, the effects of the grinding input parameter (Q_w'), the wear state of the grinding wheel (through V_w'), and the abrasive mixture on the boundary-affected layer thickness are a controversial topic. The multi-effects caused by several factors increase the dispersion of results, making difficult to isolate the contributions of each phenomenon.

4 Conclusions

The influence of sol-gel (microcrystalline) aluminum oxide grits concentration in conventional grinding wheels, as well as the process severity, evaluated by the specific material removal rate and specific material removal, was investigated. Discrepancies in the results, which could not be explained by the logic of the grinding process behavior showed a better understanding after an X-ray microtomography analysis. This analysis revealed discrepancies on the grinding wheels' pores, binder, and abrasives' content not shown in the wheel label. The grinding wheel selection for the purposed investigation considered that all the grinding wheels were manufactured with an equal phase distribution. The analysis of the results

thereafter (grinding force components and subsurface damage) were better understood after verifying content modification by the X-ray microtomography analysis, highlighting the importance of further evaluation of the grinding wheel structure.

Although the presence of microcrystalline grits on the specific grinding forces (F_t' and F_n') did not evidence a distinguishable trend, increasing the microcrystalline grit content led to a longer grinding wheel life, which in turn led to the maintenance of the grinding force for a longer period.

Increasing the specific material removal rate (Q_w') led to a more pronounced chatter at lower specific material removals (V_w') and therefore earlier grinding wheel end of life.

The boundary-affected layer formation was not mainly affected by the thermal load on the ground surface. Indications of white layer presence without dark layer hint for the formation of white layer aided by severe plastic deformation. Only a few conditions illustrated the presence of white layer accompanied of dark layer, conditions where the abrasive wear was believed to be severe, causing the flattening of the grit and thus increasing the rubbing/friction of the grit.

Increasing the microcrystalline aluminum oxide content in the grinding wheel did not present a clear trend on the boundary-affected layer thickness; however, a few hypotheses were drawn. The results suggest a shift on the predominance of the abrasive grit, from the monocrystalline to the microcrystalline with the increase of the specific material removal and/or increase of the specific material removal rate. Therefore, the boundary-affected layer thickness was likely to reflect the grinding wheel micro-wear, the abrasive grit volumetric content, and the abrasive grit properties (heat conductivity and toughness), in a combination of the material removal particularities of the external cylindrical plunge grinding.

Acknowledgments The authors would like to thank the Brazilian National Council for Scientific and Technological Development (CNPq), and the Coordination for the Improvement of Higher Education Personnel (CAPES)/*Deutsche Forschungsgemeinschaft* (DFG) – BRAGECRIM - *Technische Universität Berlin* for the financial support on the development of this project. The authors also would like to thank Guilherme Augusto Paquelin Gomes for his contributions.

References

1. Wegener K, Bleicher F, Krajnik P, Hoffmeister H-W, Brecher C (2017) Recent developments in grinding machines. CIRP Ann Manuf Technol 66:779–802
2. Oliveira JFG, Silva EJ, Guo C, Hashimoto F (2009) Industrial challenges in grinding. CIRP Ann Manuf Technol 58:663–680
3. Madopothula U, Lakshmanan V, Nimmagadda RB (2017) Time dependent behavior of alumina grains manufactured by two different routes while grinding of AISI 52100 steels. Arch Civ Mech Eng 17:400–409
4. Salonitis K (2015) Grind Hardening Process, 1st edn. Springer Cham Heidelberg New York Dordrecht, London, p 102
5. Nguyen T, Zhang LC (2011) Realisation of grinding-hardening in workpieces of curved surfaces—Part 1: Plunge cylindrical grinding. Int J Mach Tools Manuf 51:309–319
6. Lipinski D, Kacalak W, Balasz B (2019) Optimization of sequential grinding process in a fuzzy environment using genetic algorithms. J Braz Soc Mech Sci Eng 41:1–14. https://doi.org/10.1007/s40430-019-1601-6
7. Zischan D, Beizhi L, Steven LY (2016) Material phase transformation at high heating rate during grinding. Mach Sci Technol 20(2): 290–311
8. Nadolny K (2014) State of the art in production, Properties and applications of the microcrystalline sintered corundum abrasive grains. Int J Adv Manuf Technol 74:1445–1457
9. Eranki J, Xiao G, Malkin S (1992) Evaluating the performance of "seeded gel" grinding wheels. J Mater Proccess Technol 32:609–625
10. Kitamura F, Gotanda K (1992) High performance steel grinding using SG /alumina wheels. J Jpn Soc Precis Eng 58:583–585
11. Jackson MJ, Mills B (2000) Materials selection applied to vitrified alumina & CBN grinding wheels. J Mater Process Technol 108: 114–124
12. Mayer J, Engelhorn R, Bot R, Weirich T, Herwartz C, Klocke F (2006) Wear characteristics of second-phase-reinforced sol-gel corundum abrasives. Acta Mater 54:3605–3615
13. Brunner G (1998) Schleifen mit mikrokristallinem Aluminiumoxid. PhD dissertation. Universität Hannover, Germany, p 137
14. Klocke F, Engelhorn R, Mayer J (2002) Weirich T (2002) Microanalysis of the contact zone of tribologically loaded second-phase reinforced sol-gel-abrasives. CIRP Ann Manuf Technol 51:245–250
15. Fathallah BB, Fredj NB, Sidhom H, Braham C, Ichida Y (2009) Effects of abrasive type cooling mode and peripheral grinding wheel speed on the AISI D2 steel ground surface integrity. Int J Mach Tools Manuf 49:261–272
16. Madopothula U, Lakshmanan V, Nimmagadda RB (2017) Time dependent behavior of alumina grains manufactured by two different routes while grinding of AISI 52100 steels. Arch Civ Mech Eng 17:400–409
17. Madopothula U, Nimmagadda RB, Lakshmanan V (2018) Assessment of white layer in hardened AISI 52100 steel and its prediction using grinding power. Mach Sci Technol 22(2):299–319
18. Griffiths B (2001) Manufacturing surface technology. Penton Press, London, 237
19. Fang-yuan Z, Chun-zheng D, Min-jie W, Wei S (2018) White and dark layer formation mechanism in hard cutting of AISI52100 steel. J Manuf Process 32:878–887
20. Arganda-Carreras I, Kaynig V, Rueden C, Eliceiri KW, Schindelin J, Cardona A, Seung HS (2017) Trainable Weka Segmentation: a machine learning tool for microscopy pixel classification. Bioinformatics 33(15):2424–2426
21. Uhlmann E, Hasper G, Heitmüller F (2013) Verschleißmodell für Sinterkorundschleifscheiben. Werkstattstech Online 6:511–516
22. Brockhoff T (1999) Grind-hardening: a comprehensive review. CIRP Ann Manuf Technol 48:255–260
23. Shaw MC, Vyas A (1994) Heat-affected zones in grinding steel. CIRP Ann Manuf Technol 43:279–282
24. Shichao X, Minghe L, Jianhen W, Xiuming Z (2015) Study on grinding strengthening and hardening mechanism under small depth of cut conditions. Int J Surf Sci Eng 9(6):479–492

25. Linke BS (2014) Review on grinding tool wear in terms of sustainability. Proceedings of the ASME 2014 Int Manuf Sci Eng Conf Detroit, Michigan, p 9
26. Klocke F (2009) Manufacturing processes: Grinding, Honing, Lapping, vol 2. Springer-Verlag, Berlin, 452